

Acoustical Waveguide Measurements

by Justin Lawson

Advisor: Dr. John Price

REU Program CU Boulder

Introduction

This research project can be divided into two relatively independent experiments. The first deals with an attempt to simulate numerically (using Matlab) the sound field measurements made on a cylindrical waveguide setup with a horn attachment. The second is an experimental sampling of the dynamics governing air jet amplification in a recorder head. While each of these will require its own introduction, the core apparatus and certain fundamental acoustical principles are basic to both projects and it is with these that I begin.

Background

Setup:

Conventional measurements of the sound field produced by a musical instrument are typically expensive (using anechoic chambers and stressing very small microphones) or very approximate (complicated wall reflection or microphone scattering calculations being needed for exactness). The Acoustic Vector Network Analyzer (AVNA) circumvents many of these issues being constructed from readily available and relatively inexpensive materials and by mounting the microphone surfaces flush with the side of the waveguide (Fig. 1). With multiple microphones it measures both phase and attenuation information as well as the standard pressure amplitudes.

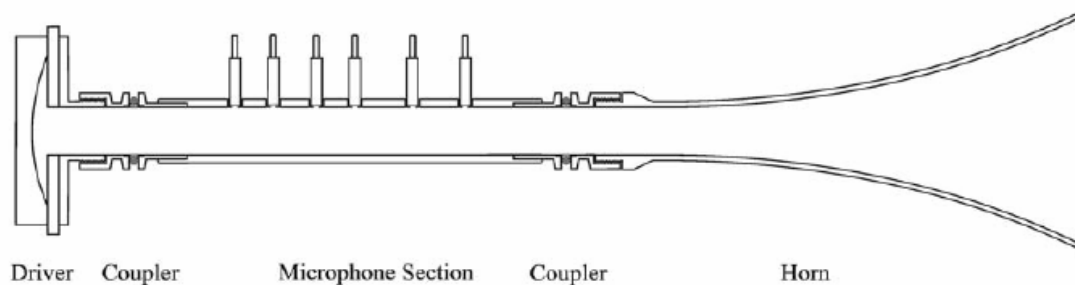


Figure 1: AVNA cross-section with horn termination

Sound waves of the desired frequency are produced by a compression driver (seen on the left in Fig. 1), designed to feed a cylindrical waveguide. The various sections are joined by ARS-25 couplers consisting of two flanges and an o-ring seal (see Fig. 2a and 2b). The electret microphone signals each pass through a buffer amplifier and are adapted to drive standard audio microphone preamplifiers. A digitizer receives these preamp signals for analysis by the computer; it also produces the driver signal. Figure 3 shows the complete layout of the apparatus.



(a)



(b)

Figure 2: (a) Two flanges and o-ring seal (b) Clasp



Figure 3: In the top left is the digitizer with six buffer amplifiers leading from each microphone. The AVNA is shown with a closed end attachment in the foreground atop two stands.

The AVNA software fits the time independent pressure amplitudes (phasors) to a right going and left going pressure wave from which the ratio of the two can be calculated and graphed to display reflection information.

Basic Theory:

The one-dimensional wave equation for a sound wave in a fluid with no elastic resistance to shear forces is given by

$$\frac{\partial^2 \xi}{\partial t^2} = \frac{K}{\rho} \frac{\partial^2 \xi}{\partial x^2} \quad \text{or} \quad \frac{\partial^2 p}{\partial t^2} = \frac{K}{\rho} \frac{\partial^2 p}{\partial x^2} \quad (1)$$

where ξ is the displacement of the medium and p is the pressure. The velocity of the wave, c , is then given by $c = (K/\rho)^{1/2}$ where K is the bulk modulus (roughly, the constant of proportionality between volume and pressure changes; specific to the medium) and ρ is the density of the medium.

At a rigid boundary we expect the normal velocity of the fluid to be zero or, equivalently, the normal force (which goes like the normal component of the pressure gradient) to be zero, that is,

$$\frac{\partial \xi}{\partial t} = 0 \quad \text{or} \quad \hat{n} \cdot \nabla p = 0 \quad (2)$$

Generalizing equations (1) and (2) to three dimensions and solving the boundary value problem for a cylindrical waveguide we find that a pressure wave must propagate with m angular nodes and n radial nodes (temporarily assuming an infinite axial direction where boundary conditions will eventually vary with the end attachments used). The first four propagating modes (m,n) are shown below in Figure 4.

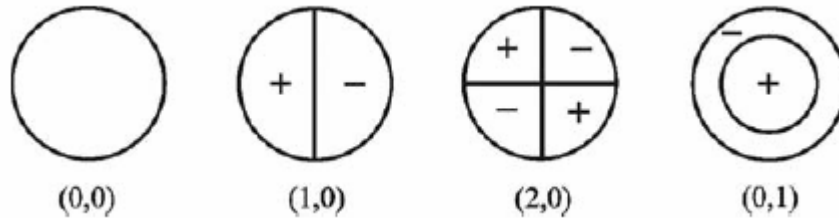


Figure 4: First four propagating pressure modes (m,n)

Where oscillating time solutions are assumed ($p \sim e^{i\omega t}$), we find that the cutoff frequency for each mode is given by

$$\omega_c = \frac{\pi q_{mn} c}{a} \quad (3)$$

q_{mn} is the n th zero of the m th Bessel function and a is the radius of the waveguide. Below ω_c , a mode will decay exponentially along the axis.

Using the dimensions of the AVNA setup ($a = 1.25\text{cm}$) we find that the second lowest mode to propagate (1,0) does not do so until 8kHz (the lowest (plane) mode propagates for all frequencies ($\omega_c = 0$)) which is well beyond the frequency range of interest for most musical instruments (50 to 3000Hz). Thus for all but the most extreme cases, the microphone measurement at the cylinder walls reflect the pressure along the entire plane perpendicular to the axis at that point.

If we wish to represent end attachments in the boundary value problem, it pays to discuss the acoustical impedance, Z , given by the pressure divided by the volume flow, $Z = p(x,t)/U(x,t)$,

where p and U are analogous to voltage and current respectively in the electrical case. As in the simple optical reflection problem, different acoustic regimes (differing in geometry or medium properties) are characterized by different impedances as different optical media are characterized by different indices of refraction (see Figure 5).

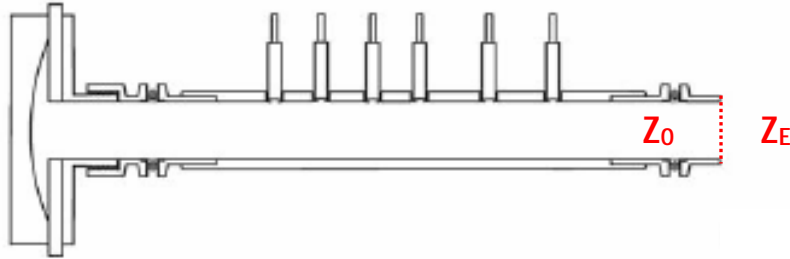


Figure 5: Cylindrical waveguide reflection problem

Here Z_0 is the characteristic impedance of the cylinder (given by $\rho c/S$ where $S = \pi a^2$) and Z_E is the termination or end impedance. The pressure in the pipe can be represented as a superposition of a left going and right going wave as can the volume flow

$$p(x,t) = [Ae^{-ikx} + Be^{ikx}]e^{iot} \quad (4)$$

$$U(x,t) = [Ae^{-ikx} - Be^{ikx}]e^{iot} \quad (5)$$

(volume flow is measured as positive to the right thus the minus sign before the left going amplitude). From this and the definition of the impedance we can calculate the ratio of the left and right going pressure waves

$$\frac{Be^{ikx}}{Ae^{-ikx}} = \frac{(Z_E - Z_0)}{(Z_E + Z_0)} \quad (6)$$

where x in this case is evaluated at the reflection plane.

Horn Simulation

The simplest end attachments are the closed end (rigid end boundary) and open end (no boundary) whose impedances we expect to be $Z_E = \infty$ (no volume flow, $U=0$) and 0 (infinite cross section, S) respectively. The ratio of left and right going waves – henceforth \tilde{R} or the reflection coefficient (although conventionally this term is reserved for intensity ratios we will never discuss these in this paper) – from (6) we expect to be 1 and -1 respectively. Figure 6

below shows a plot of \tilde{R} on the complex plane which, to within the range of experimental error, can be said to agree with the theoretical prediction of one.

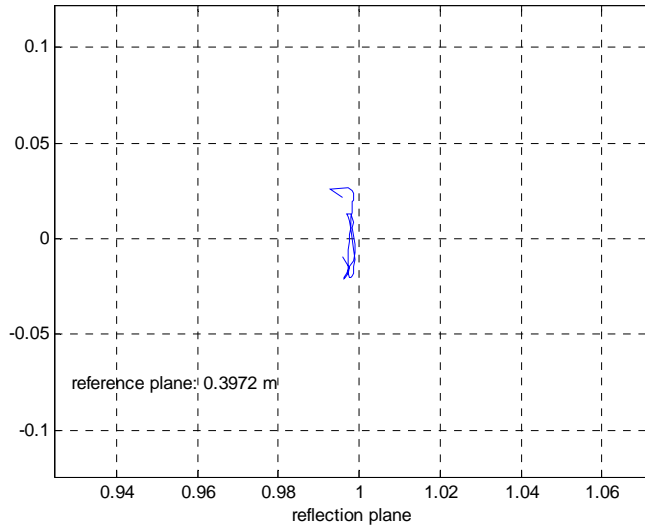


Figure 6: Reflection plane for closed end attachment

The agreement is not so close, however, for the open ended case. This is because the impedance in open space for a sound wave is not exactly zero, but has some finite value which, although much smaller than the Z_0 , is not negligible. Figure 7a shows the reflection plane for an unflanged open end while 7b shows the absolute value of the reflection coefficient (top) and phase (bottom) versus frequency.

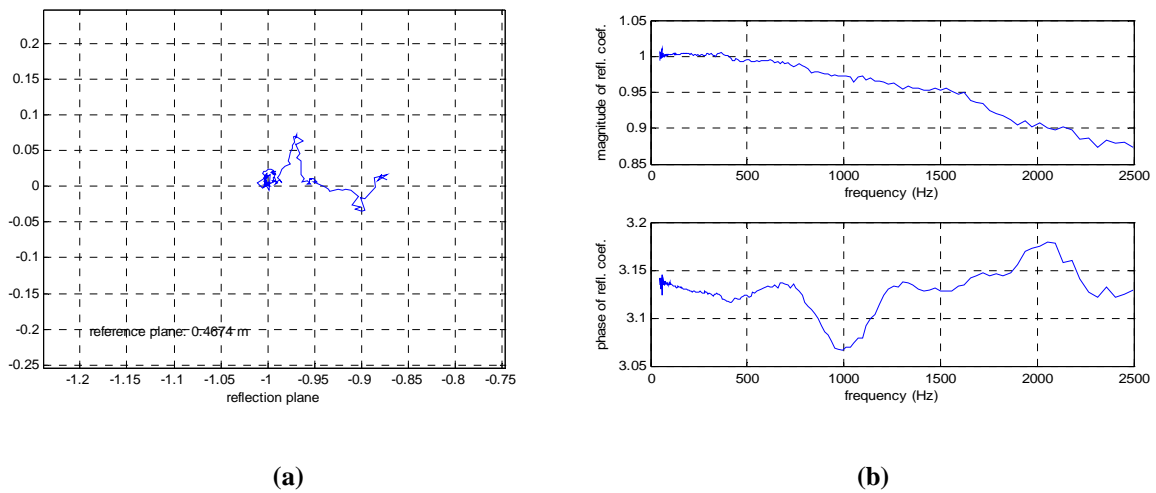


Figure 7: (a) \tilde{R} plotted on the complex plane (b) magnitude of \tilde{R} and phase vs. frequency

Of particular interest is the steady decline of the magnitude of \tilde{R} as a function of frequency and the fact that the reflection plane must be shifted by 0.702cm (theory predicts 0.76cm) from its actual physical end such that the reflection coefficient agrees with the ideal case ($Z_E=0$). With the added complexity of an open ended attachment, theory becomes highly approximate and it makes sense to numerically simulate the results for comparative purposes.

First we wish to simulate the infinite space in which the sound wave propagates beyond the waveguide. We model this as a large sphere with sound absorbing walls. The condition for absorption, from (6), is that $Z_I = Z_S$ where the impedance inside the sphere is equal to that on the sphere. At a large radius, the sound wave is approximately planar and a plane wave has impedance $Z = \rho c$ (in code we set ρ and c equal to one). Using the following relation between pressure and volume flow assuming oscillatory time dependence and $Z=p/U$

$$\vec{U} = \frac{i}{\omega\rho} \nabla \vec{p} \quad (7)$$

and $Z=p/U=1$ we obtain the boundary condition

$$\hat{n} \bullet \nabla \vec{p} + ik\vec{p} = 0 \quad (8)$$

(equation (7) is nothing more than Newton's equation where the negative pressure gradient represents the force and the time derivative of U the acceleration).

To test this absorbing-sphere approximation of infinite space we calculate numerically for the simple case of a pulsating sphere (which has an analytical closed form solution). The PDE toolbox of Matlab allows us to draw such a geometry by hand in the graphical user interface (GUI) as well as define boundary conditions along its edges, mesh the geometry and solve the PDE at the intersections of the resulting mesh-grid. Figure 8 shows the meshed geometry for the pulsating sphere case.

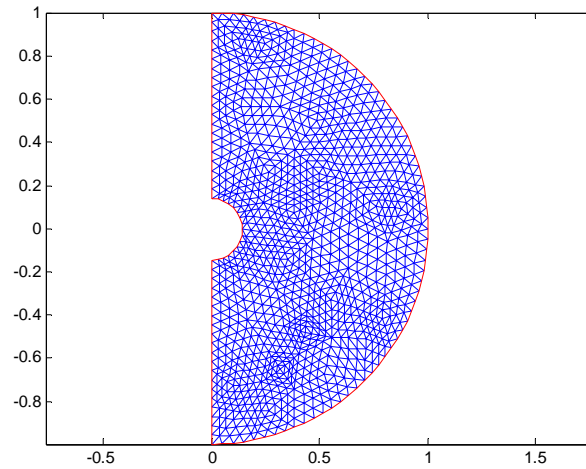


Figure 8: Meshed geometry for pulsating sphere surrounded by an absorbing radius (to be rotated about the y axis).

The standard two-dimensional Cartesian wave equation has been modified (appropriate coefficients chosen and angular symmetry conditions (periodic BC's) imposed) to represent the 3D cylindrical case ($y=z$ and $x=r$ in Fig. 8 above). The remaining boundary conditions are $\hat{n} \cdot \nabla \bar{p} = 1$ for the driver (amounts to a velocity condition: sound wave traveling at $c=1$ from the speaker) and $\hat{n} \cdot \nabla \bar{p} = 0$ on the axis of rotation ($y=0$ above) amounting to a C^1 continuity condition. Solving for this in the GUI we receive the 3D plot (with pressure as the third axis) of Figure 9.

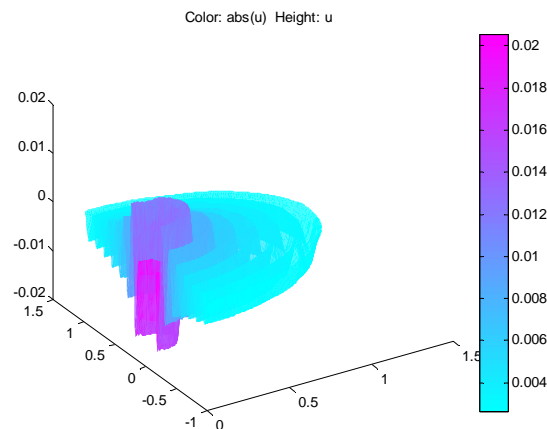


Figure 9: Pressure (height) vs. z and r

Theory predicts oscillating radial solutions that decay like $1/r$ ($p \sim p_0 \frac{e^{-ikr}}{r}$). To compare the numerical and analytical solutions, we write a program to average all solution values within a certain radial bin (of width dr) and plot average pressure vs. r (as seen in Figure 10 below). (Matlab's interpolation functions do not work unless the mesh is excessively fine). See appendix A for more information on this simulation.

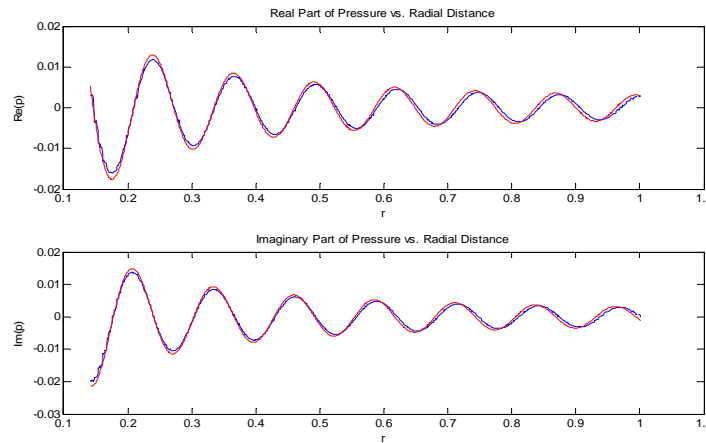


Figure 10: p vs. r . Theoretical in red, numerical in blue

The theoretical and simulated results seem to agree nicely.

To represent more abstract geometries or to define exact proportions (in the GUI a circle can only be drawn to have *approximately* the desired radius) the GUI is no longer useful and geometry and boundary value programs must be written which use some of the PDE toolbox's underlying inbuilt functions. For more information on these programs see appendix B.

Constructing a geometry which attaches the absorbing sphere to the open end of the waveguide and following a procedure similar to that above (using command line functions instead of the GUI), we obtain the following geometry (Figure 11) and coefficient of reflection data (Figure 12).

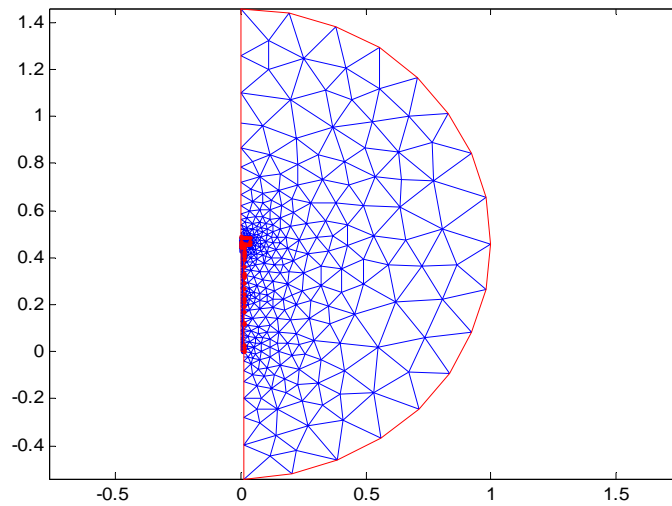
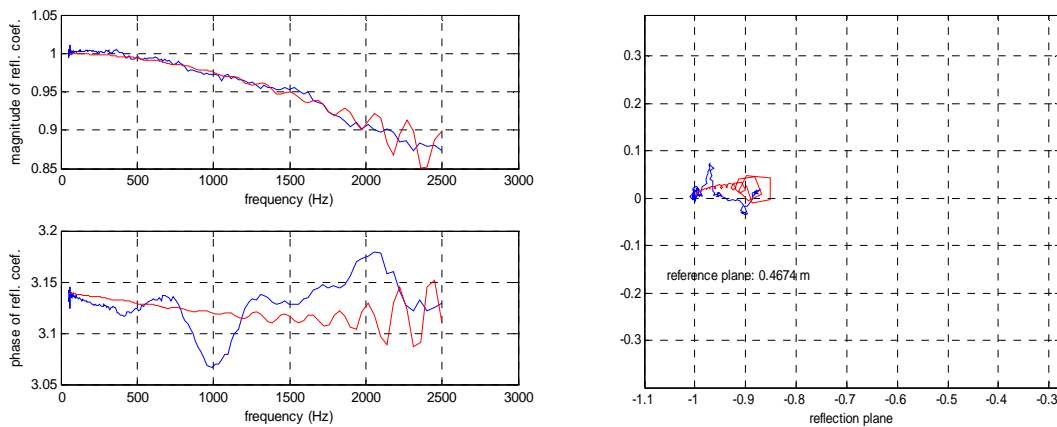


Figure 11: Open ended pipe geometry



**Figure 12: Numerical (red) vs. experimental (blue) reflection data
(compare with Figure 7)**

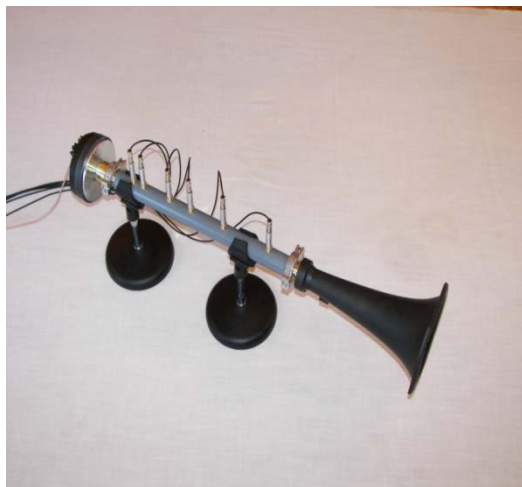
Note in Figure 11 a small box around the tube end (this will become more prominent in the horn simulation below); this is used to divide the geometry into two regions for which different mesh fineness is desired (we care less about the precision of the solution in the absorbing sphere than inside the tube where the data is actually taken in the experiment). Boundary condition (2) is used for the pipe walls and the constant velocity condition used for the pulsating sphere is imposed for the compression driver boundary.

The overall downward trend of the reflection magnitude agrees well with the experimental data as does the end correction to the reflection plane (the model behaves as if the

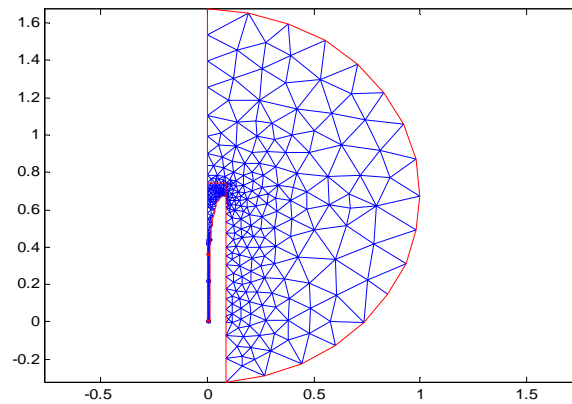
pipe were roughly 0.7cm longer in the idealized case). Not accounted for experimentally, however, is the ringing of both magnitude and phase at larger frequencies. This, we have come to conclude, is because the ringing is simply too small to observe for the open ended case and is lost in noise.

Ultimately, we hoped to model a horn attachment to the open pipe which, fortunately, exaggerates these ringing and damping effects to a level beyond apparatus noise. The period of the ringing is proportional to the end radius which is much larger for a flaring horn (we should observe broader oscillations). A horn is also designed to radiate meaning the reflection magnitude will drop more dramatically (at certain frequencies to near zero) and begin to do so at a lower frequency.

Following a similar procedure to that for the open end (only the geometry changes, not the boundary conditions), we achieve the meshed geometry shown in Figure 13b (compare with real setup 13a) and the numerical (red) vs. experimental (blue) reflection data displayed by Figure 14 below.



(a)



(b)

Figure 13: (a) Experimental setup (b) Matlab geometry

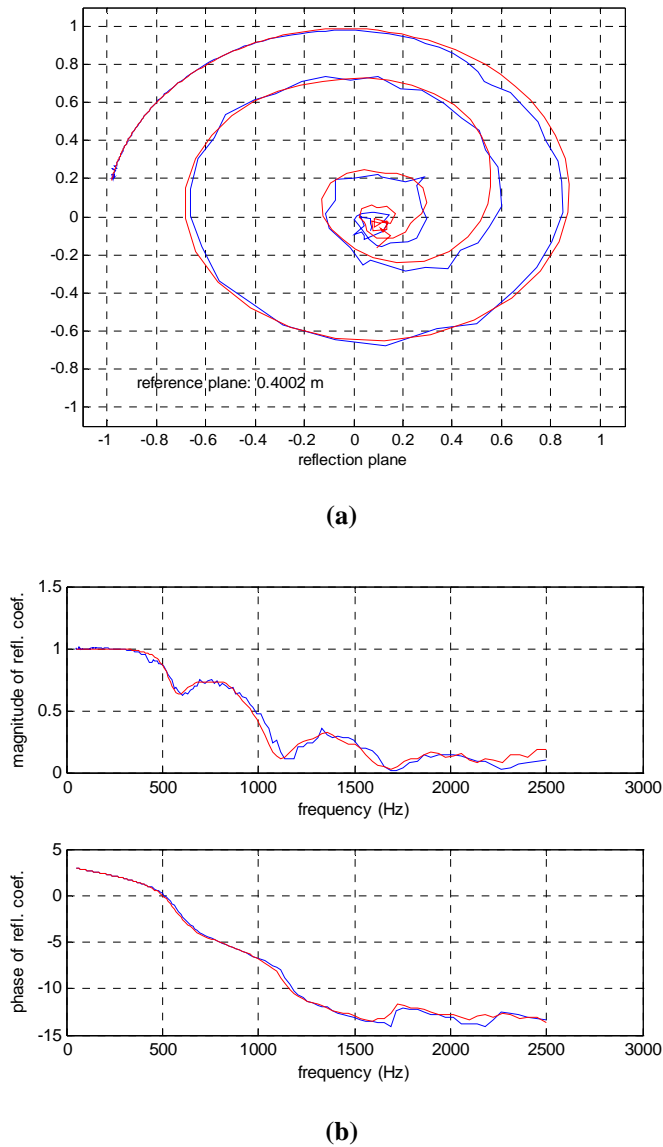


Figure 14: (a) Reflection plane for horn attachment
(b) Magnitude (top) and phase (bottom) of \tilde{R}

As expected, the ringing period is notably lengthened and the drop in the reflection ratio's magnitude comes sooner and more abruptly. The numerical simulation on Matlab matches these features nicely. Again for more information on the detailed workings of this program see appendix B.

Air Jet Amplification of a Recorder Head

Background

Rayleigh calculates that a disturbance in an air jet will propagate with half the jet speed and will grow exponentially with time along the jet. Such a disturbance is caused in a recorder where an air jet emerging from the flue-slit (part B in Figure 15) is moved by an oscillating flow from the air column (the tube on the recorder), the oscillating air flow can be written as

$$h_1 = -i \left(\frac{v}{\omega} \right) e^{i\omega t} \quad (9)$$

where v is the flow velocity, ω its frequency and h_1 the vertical disturbance of the jet. In itself, this flow (which is constant over the opening) would simply move the entire jet up and down, but the jet is constrained by the flue-slit, thus, the vertical disturbance here must be zero and another term must be added to (9). It is this term that propagates along the air jet causing it to oscillate about the sharp edge (part C of Figure 15) and inject a volume flow into the air column.

$$h(x) = -i \left(\frac{v}{\omega} \right) \left\{ \exp i\omega t - \exp \mu t \exp \left[i\omega \left(t - \frac{x}{u} \right) \right] \right\} \quad (10)$$

Here μ is the disturbance growth constant and u is the disturbance velocity. The injected volume flow from the air jet occurs at the same frequency as the original column flow, the net effect of the recorder head is to amplify the incoming signal and create a sustained oscillation if multiple passes are allowed (reflections back from the open end).

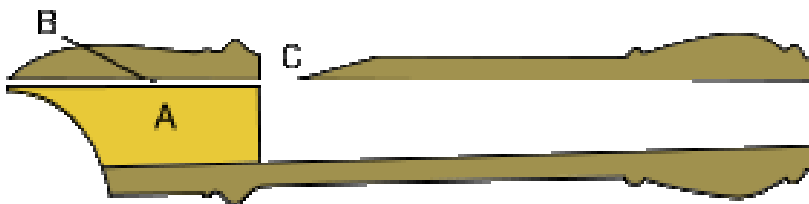


Figure 15: Recorder head cross section

Experiment

The objective of this experiment was to measure the amplification (single pass) of an incoming signal by the recorder head. We expect the amplification to vary as a function of the signal frequency, ω , and the air jet velocity ($2u$) which is determined by the pressure applied to the mouth. We wish to prevent sustained oscillations such that the right going wave (away from the driver) is only that imposed by the driver and the left going wave a mixture of the reflected wave and the air jet volume flow.

To prevent multiple passes (i.e. a twice reflected component traveling right) we construct an attenuator after the driver and before the microphone section (see the cross section below in Figure 16). This is accomplished by stuffing a tube section with cotton. Pressure flow to the recorder mouth is controlled using a vinyl tubing setup running from a compressed air valve through an attenuating valve into a buffer volume and into the recorder mouth. A manometer attached in parallel to the setup measures the applied pressure in mmH₂O (1mmH₂O ≈ 10pascal).

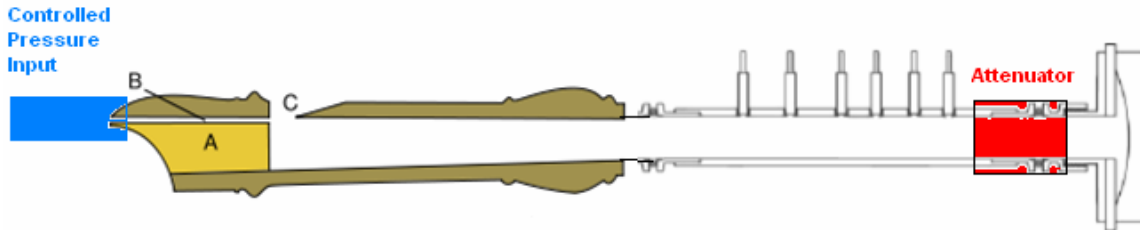
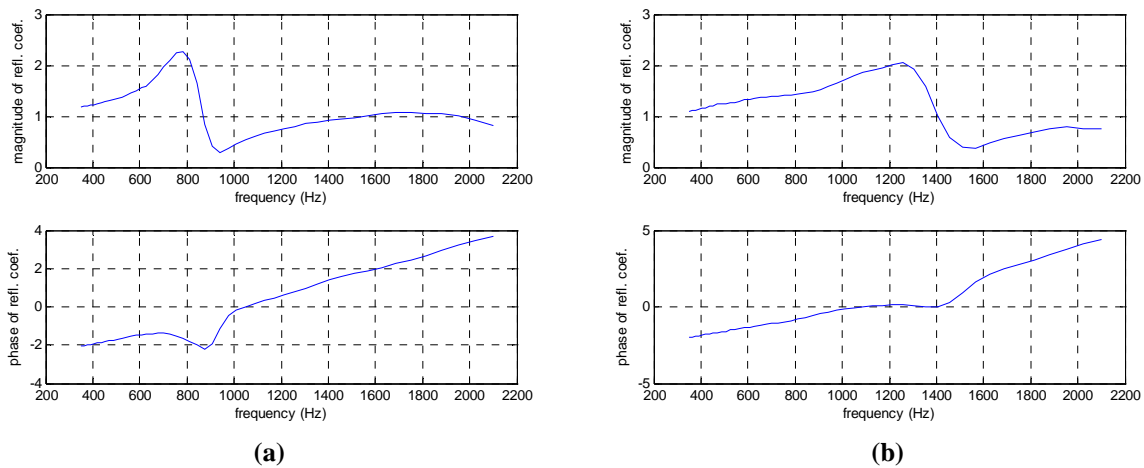
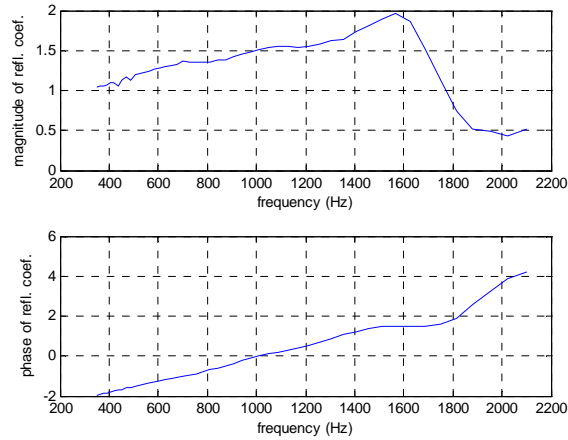


Figure 16: Experimental setup cross section

Accuracy of the manometer was good to roughly $\pm 0.5\text{mm}$. Thirteen test runs were made varying from 11 to 53mmH₂O air pressure (experimentally the range appears to lie between 3 and 85mmH₂O) with steps between 3 and 4mm (it is recommended for more accurate testing that the manometer be tilted at some small angle from the horizontal and the water-level reading be multiplied by the sine of the angle). The input signal ranged from 350 to 2100Hz which is roughly the span for the alto recorder. Figure 17 below shows three graphs of the reflection coefficient magnitude and phase versus frequency for blowing pressures 14, 29 and 45mmH₂O.





(c)

**Figure 18: Reflection magnitude and phase data vs. frequency
For 14 (a), 29(b) and 45mmH₂O (c)**

As will be noted from the figures, for each blowing pressure there is a frequency of maximum response (resonance) which occurs at larger frequencies for larger blowing pressures (high note resonances require greater air pressure). The net amplification at this resonance frequency decreases slightly as a function of blowing pressure, yet remains roughly around a factor of two within the recorder range. Deviating slightly from this frequency, the recorder head has a damping effect (we expect a magnitude of one without the air jet since the recorder behaves approximately like an open end in this configuration). In the low and high frequency limits the reflection magnitude approaches one signifying little to no amplification. Also of interest is the relative broadening of the amplifier's spike and dip as blowing pressure is increased. (Pressure resolution was not sufficiently high to plot reflection data as a function of blowing pressure. General trends however can be ascertained from the graphs above). For more information on these data files see Appendix C. For information on air jet amplifier theory see Fletcher in references.

Appendices

For all of the programs below, knowledge regarding basic pdetool operation and AVNA software use is assumed. For additional information on these topics see Matlab help and the AVNA Users Guide respectively.

Appendix A

sphericalpulser.m

Simply run this program to reproduce the meshed geometry and pressure solution results of figures 8 and 9.

rvpplotter.m

The Matlab program rvpplotter requires no inputs. It does, however, require you to load both mesh information (variables p, e and t) as well as the solution values (u in pdetool) into the workspace after running sphericalpulser.m. This can be done easily in the pdetool GUI by clicking on the Mesh and Solve menus.

The pdetool solver stores x and y values as the first and second rows of the mesh matrix p; rvpplotter calculates the values for r (spherical radial distance) by $r = (x^2 + y^2)^{1/2}$. It then finds the location (in the p matrix) of all r values within a certain range (r to r+dr) and averages the corresponding u values. The program runs from the smallest r value (in our case the pulsing sphere radius) to its largest value (the absorbing sphere radius). After the binning procedure has run over all r's rvpplotter plots u vs. r alongside the theoretically calculated pressure which goes like an oscillating term over r.

While it may seem easier to use one of Matlab's inbuilt interpolation functions to achieve these results, an extremely fine mesh is required to achieve results similar to figure 10. Running such a mesh takes a good deal of time.

Appendix B

defaults.m

Similar to the defaults.m of the AVNA software this file stores all parameter values (i.e. mic locations, pipe length etc.). See the program for an explanation of each parameter.

hornling.m

For more complex geometries or to input exact dimensions, the GUI cannot be used and a program describing the desired geometry must be written. hornling.m offers two methods for inputting the geometry. A set of measured data points can be input into the defaults file in which

case matlab will interpolate between points for meshing purposes or an analytical function can be defined for the horn geometry (in the function file `geo.m`).

Both the open end and the horn can be simulated using this file where the geometry is simply altered to fit each end attachment. The geometry function `hornling.m` is used by the inbuilt PDE solve function (you will never type it in the command line) thus its inputs, `bs` and `s`, need not concern us. For additional help see `pdegeom` in Matlab help and comments in the program.

geo.m

This function file defines the two methods mentioned above in the geometry program `hornling.m`. This is where the user can alter the analytical function defining horn geometry or the method of interpolation from the measured data in `defaults.m`

hornsolvemult.m

The following matlab program meshes the geometry defined in `hornling.m` then solves at the mesh points for a range of `k` values defined in the input arguments. It then interpolates from the solution values onto a grid of specified axial values (for this case we use the microphone positions from the experiment). The output datafile can then be fed into the `wavefit.m` program of the AVNA software whose output may, in turn, pass through the `reflect.m` program for reflection graphs. For additional information on constructing a boundary value matrix see `assemb` in Matlab help and see `assembpde` for more information on the general format of this program.

compare.m

This file comparing two wave solutions (for example Figure14) is only a slightly modified version of the AVNA file `reflect.m`.

Appendix C

All data files for the air jet amplifier experiment are stored as `'datrec(pressure value)mm'` where pressure value is a number such as 11 (i.e. `'datrec11mm'`). Wave files are saved as `'wavrec(pressure value)mm'` and reflection files as `'reflrec(pressure value)mm'`.

References

1. Fletcher, Neville H. and Rossing, Thomas D. The Physics of Musical Instruments. Springer-Verlag New York Inc. 1991.
2. Price, John. Acoustic Waveguides. University of Colorado, Boulder. 2008.
3. Price, John. AVNA User's Guide. University of Colorado, Boulder. 2008.